Improved low-resolution crystallographic refinement with Phenix and Rosetta

Frank DiMaio[1,6], Nathaniel Echols[2,6], Jeffrey J Headd[2], Thomas C Terwilliger[3], Paul D Adams[2,4] & David Baker[1,5]

Refinement of macromolecular structures against low-resolution crystallographic data is limited by the ability of current methods to converge on a structure with realistic geometry. We developed a low-resolution crystallographic refinement method that combines the Rosetta sampling methodology and energy function with reciprocal-space X-ray refinement in Phenix. On a set of difficult low-resolution cases, the method yielded improved model geometry and lower free R factors than alternate refinement methods.

While determination of X-ray crystal structures at moderate to high resolutions has recently accelerated, structure determination and refinement at lower resolutions remains problematic[1] despite considerable recent work[2–8]. We reasoned that combining the strengths of the Rosetta structure modeling methodology and the Phenix X-ray refinement software could yield improved refinement at low resolution. Rosetta utilizes a detailed all-atom force field that could partially compensate for the lack of high-resolution data, as well as search procedures combining backbone minimization with discrete side-chain optimization that more effectively explore alternative side-chain arrangements than does simulated annealing. Phenix is a state-of-the-art X-ray refinement package that can be readily integrated with other computational methods. We therefore incorporated the maximum-likelihood reciprocal-space X-ray target function from phenix.refine[9] into Rosetta.

To enable refinement in Rosetta, we use Phenix routines (called through Python bindings) to calculate the crystallographic refinement target function. Rosetta energy is weighted against the crystallographic likelihood function by normalizing the gradients of each before each minimization cycle[10]. Unlike in standard Rosetta structure prediction, non-ideal bond geometry is allowed throughout refinement; Rosetta symmetry[11] optimizes the energy of the protein in the crystal lattice. The combined approach (phenix.rosetta_refine) uses Phenix[12] to perform bulk solvent correction, calculate electron-density maps and refine B factors, while the Rosetta force field, minimizer and sampling methods optimize model geometry. Modular interfaces to the new refinement protocols provided by RosettaScripts[13] and Phenix allow refinement protocols to be customized (**Supplementary Figs. 1**–**3**).

Using this framework, we developed a protocol to optimize poor starting models against low-resolution data. The method alternates real- and reciprocal-space refinement: the Rosetta force field constrains reciprocal-space refinement to physically plausible conformations; density maps restrain Rosetta side-chain and backbone sampling in real space. Significant backbone movement occurs during internal coordinate minimization, while side-chain optimization allows traversal of large energy barriers that impede traditional continuous refinement.

To assess the performance of our approach in realistic difficult cases, we assembled a collection of 26 starting models for 15 data sets at 3.0- to 4.5-Å resolution (**Supplementary Table 1**) by performing molecular replacement with low-resolution data sets using templates with nontrivial conformational changes. These cases are within the radius of convergence of molecular replacement but are far enough from the final structure that large errors were expected unless extensive manual rebuilding was applied.

We compared Rosetta-Phenix refinement (phenix.rosetta_refine) to three different low-resolution refinement strategies. As a control, structures were refined for 20 cycles in *phenix.refine*, optimizing X-ray weight at each cycle. We also refined structures in CNS[14], using the DEN methodology (with full weight optimization)[2], and in REFMAC5 (ref. 15) with jelly-body refinement. We compared the generated structures using free R factor (R_{free}), MolProbity score[16] and r.m.s. deviation to the re-refined published structure. Running times of DEN and Rosetta-Phenix were similar (about 4 h per model for a 1,000-residue protein), with Phenix roughly 4 times faster and REFMAC5 about 30 times faster (not accounting for parallelization).

The results (**Fig. 1**, **Supplementary Tables 2** and **3**) show clear improvement for CNS-DEN and REFMAC5 compared to conventional refinement in Phenix, and further improvement with Rosetta-Phenix refinement. Although DEN and REFMAC5 refinement consistently showed a large radius of convergence, model quality (using MolProbity) was worse than that of Rosetta-Phenix in all but two cases. We discuss several illustrative examples below.

The starting molecular replacement models for a Ca^{2+} ATPase structure (PDB 3FPS) require significant conformational changes

[1]Department of Biochemistry, University of Washington, Seattle, Washington, USA. [2]Physical Biosciences Division, Lawrence Berkeley National Laboratory, Berkeley, California, USA. [3]Bioscience Division, Los Alamos National Laboratory, Los Alamos, New Mexico, USA. [4]Department of Bioengineering, University of California Berkeley, Berkeley, California, USA. [5]Howard Hughes Medical Institute, University of Washington, Seattle, Washington, USA. [6]These authors contributed equally to this work. Correspondence should be addressed to F.D. (dimaio@u.washington.edu) or N.E. (nechols@lbl.gov).
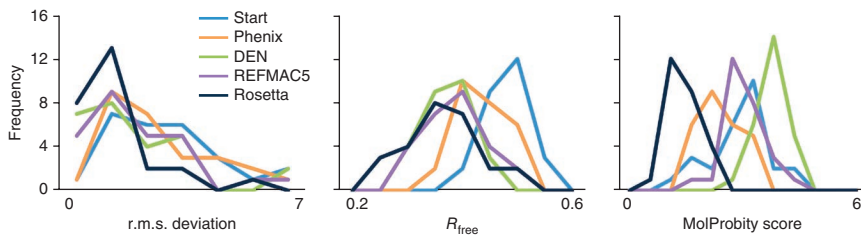
Figure 1 | Comparison of Phenix, CNS-DEN, REFMAC5 and Rosetta-Phenix refinements on a realistic low-resolution test set of 15 proteins (**Supplementary Table 1**). Histograms of the r.m.s. deviation to the deposited structure (left), R_{free} (middle), and MolProbity score, indicating stereochemical quality (right), after refinement of low-resolution test models. Starting model distributions are in blue. Source data for this figure are provided in **Supplementary Tables 2** and **3**.

to match the published structure; initial R_{free} factors are >0.5. Neither phenix.refine, DEN nor REFMAC5 was able to improve the models beyond an R_{free} of 0.43 or r.m.s. deviation of 6.0 Å. However, Rosetta-Phenix refinement starting from the conformation in the absence of calcium (PDB 2ZBG) resulted in a greatly improved fit to the data: R_{free} = 0.28 with an r.m.s. deviation of 1.68 Å to the published structure (**Fig. 2**).

The starting models for a glutamate receptor (PDB 1ISR) differ from the native structure by large hinge motions. Both CNS-DEN and Rosetta-Phenix outperformed conventional refinement; the Rosetta-Phenix model is nearly identical to the published structure (r.m.s. deviation = 0.5 Å), but with superior geometry. The final Rosetta-Phenix model starting from the ligand-free

conformation (PDB 1EWT) has an R_{free} below that of the published structure (see **Supplementary Tables 2** and **3**), despite a starting-model r.m.s. deviation of 4.5 Å.

For calcium-calmodulin-dependent protein kinase II (PDB 3KK9), CNS-DEN and Rosetta-Phenix yielded similar R factors, with the DEN model closer to the published structure. To evaluate whether a combined protocol would yield further improvement, we ran Rosetta-Phenix refinement on the DEN model; this reduced R_{free} to 0.31 (below the published structure) and corrected most of the geometry errors (**Supplementary Table 4**). This suggests that a combination of strategies may be most appropriate in some difficult cases, as the restraint data used by the methods—DEN drawing off homologous structures and Rosetta using detailed physical chemistry—are largely orthogonal.

We had used a preliminary version of our Rosetta-Phenix refinement to solve the structure of the TRIP8b channel subunit[17]. Standard refinement reduced the R_{free} slightly, but model geometry was poor. Rosetta-Phenix refinement followed by rebuilding in Coot[18] improved R_{free} from 0.46 to 0.28 while also maintaining reasonable model geometry[17] (**Supplementary Fig. 4**).

The refinement protocol described here differs from previously described refinement methods[2,6–8] in several key aspects. First, the Rosetta energy function ensures that the protein conformation remains physically plausible even when models undergo large conformational rearrangement during refinement[19]. Second, Rosetta refinement makes use of discrete side-chain optimization, which allows for large-scale reorganization of side-chain geometry not achievable through minimization alone.

Our results using the DEN method in CNS and jelly-body restraints in REFMAC5 show that reference model–derived restraints are quite powerful in low-resolution refinement. Although these methods extend the radius of convergence[2], they are less effective at improving model geometry[20]. In contrast to reference structure–based restraints, the Rosetta force field makes it possible to discover
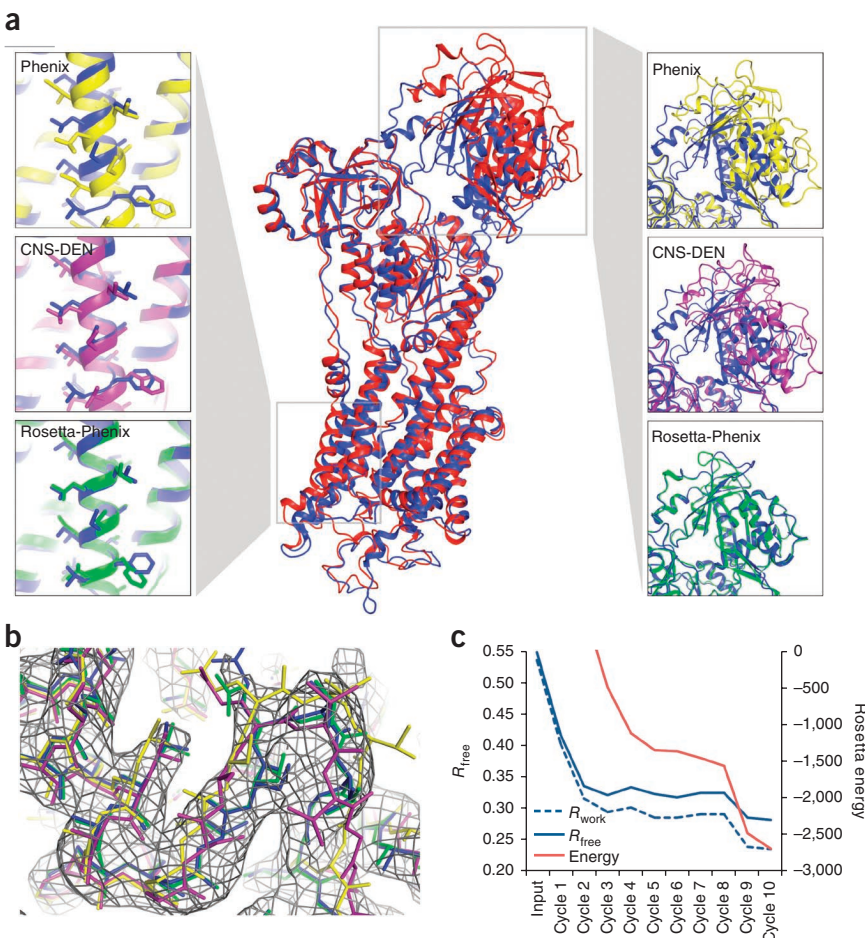

Figure 2 | Refinement of the Ca^{2+} ATPase (PDB 3FPS, PDB 2ZBG) using Rosetta-Phenix. (**a**) Alpha-carbon traces comparing the results of refinement of a molecular replacement (MR) model using rigid-body refinement (red), Phenix (yellow), CNS-DEN (purple) and Rosetta-Phenix (green); the published structure is in blue. (**b**) Close-up showing all non-hydrogen atoms (colored as above), with $2mF_o – DF_c$ electron density for the final structure contoured at 1σ. (**c**) Decrease in Rosetta energy and R_{work} and R_{free} to the deposited structure during Rosetta-Phenix refinement.

new energetically favorable interactions—not present in the reference model—during a refinement trajectory. As suggested by the results for PDB 3KK9, the combination of these approaches can be quite powerful.

We found that the combined Rosetta-Phenix method outperforms conventional refinement methods against low-resolution crystallographic data. Importantly, the method also does not degrade high-resolution structures: a high-resolution benchmark (**Supplementary Table 5** and **Supplementary Fig. 5**) showed that Rosetta-Phenix refinement produced little change in R_{free} but improved MolProbity score. Further low-resolution improvements may be achievable by incorporating the fragment-based backbone rebuilding essential to Rosetta *de novo* structure prediction and to MR-Rosetta[21].

The combined Rosetta-Phenix method requires installation of both Rosetta (version 3.6 or newer, available at https://www.rosettacommons.org) and Phenix (version 1.8.3 or newer, available at http://www.phenix-online.org), which are freely available to academics. The program *phenix.rosetta_refine* (distributed with Phenix) automates the process. All structures used for testing may be downloaded at http://www.phenix-online.org/phenix_data.

METHODS

Methods and any associated references are available in the online version of the paper.

Note: Any Supplementary Information and Source Data files are available in the online version of the paper.

AUTHOR CONTRIBUTIONS

F.D., N.E., T.C.T., P.D.A. and D.B. designed the research; F.D., N.E. and J.J.H. performed the experiments; F.D. and N.E. wrote the manuscript, and all authors edited and read the final manuscript; P.D.A. and D.B. supervised the project.

COMPETING FINANCIAL INTERESTS

The authors declare no competing financial interests.

1. Brünger, A.T., DeLaBarre, B., Davies, J.M. & Weis, W.I. *Acta Crystallogr. D Biol. Crystallogr.* **65**, 128–133 (2009).
2. Schröder, G.F., Levitt, M. & Brünger, A.T. *Nature* **464**, 1218–1222 (2010).
3. Fenn, T.D. & Schnieders, M.J. *Acta Crystallogr. D Biol. Crystallogr.* **67**, 957–965 (2011).
4. Haddadian, E.J. *et al. Biophys. J.* **101**, 899–909 (2011).
5. Koparde, V.N., Scarsdale, J.N. & Kellogg, G.E. *PLoS ONE* **6**, e15920 (2011).
6. Headd, J.J. *et al. Acta Crystallogr. D Biol. Crystallogr.* **68**, 381–390 (2012).
7. Nicholls, R.A., Long, F. & Murshudov, G.N. *Acta Crystallogr. D Biol. Crystallogr.* **68**, 404–417 (2012).
8. Smart, O.S. *et al. Acta Crystallogr. D Biol. Crystallogr.* **68**, 368–380 (2012).
9. Afonine, P.V. *et al. Acta Crystallogr. D Biol. Crystallogr.* **68**, 352–367 (2012).
10. Adams, P.D., Pannu, N.S., Read, R.J. & Brünger, A.T. *Proc. Natl. Acad. Sci. USA* **94**, 5018–5023 (1997).
11. DiMaio, F., Leaver-Fay, A., Bradley, P., Baker, D. & Andre, I. *PLoS ONE* **6**, e20450 (2011).
12. Adams, P.D. *et al. Acta Crystallogr. D Biol. Crystallogr.* **66**, 213–221 (2010).
13. Fleishman, S.J. *et al. PLoS ONE* **6**, e20161 (2011).
14. Brünger, A.T. *et al. Acta Crystallogr. D Biol. Crystallogr.* **54**, 905–921 (1998).
15. Murshudov, G.N. *et al. Acta Crystallogr. D Biol. Crystallogr.* **67**, 355–367 (2011).
16. Chen, V.B. *et al. Acta Crystallogr. D Biol. Crystallogr.* **66**, 12–21 (2010).
17. Bankston, J.R. *et al. Proc. Natl. Acad. Sci. USA* **109**, 7899–7904 (2012).
18. Emsley, P., Lohkamp, B., Scott, W.G. & Cowtan, K. *Acta Crystallogr. D Biol. Crystallogr.* **66**, 486–501 (2010).
19. Das, R. & Baker, D. *Annu. Rev. Biochem.* **77**, 363–382 (2008).
20. Brünger, A.T. *et al. Acta Crystallogr. D Biol. Crystallogr.* **68**, 391–403 (2012).
21. DiMaio, F. *et al. Nature* **473**, 540–543 (2011).

ONLINE METHODS

Generation of test cases. Structures and crystallographic data were selected based on resolution, the absence of non-crystallographic symmetry and the availability of related structures to be used as search models for molecular replacement. Suitable MR models were identified with an r.m.s. deviation between 1.5 Å and 4.5 Å to the final deposited structure, and starting models for refinement were generated by molecular replacement in Phaser[22] after minimal trimming of loops and terminal regions not found in the target structure. The search models for PDB 3IDQ, 3A8N and 3SNH were processed by the Sculptor program[23] to match the sequence of the target. Where necessary, crystallographic symmetry operators and origin shifts were applied using phenix.find_alt_orig_sym_mate[24] to place the MR solution in the same frame of reference as the published structure.

Rosetta flexible bond geometry and Cartesian refinement. During internal coordinate refinement, both bond angles and bond lengths were allowed to deviate from their ideal values. Harmonic potentials were added to restrain both bond angles and bond lengths; planarity was enforced using pseudotorsional restraints. Cartesian-space refinement was implemented using the same harmonic restraints and was found to produce significant improvement in structure optimization against the data while simultaneously improving model geometry. Both minimization strategies can be used and modified via RosettaScripts[13].

Rosetta refinement strategy. Rosetta was compiled with a Python interpreter that directly calls Phenix functions using C++ Python bindings[25]. Phenix functionality was used to perform bulk solvent correction and anisotropic scaling[26] and to calculate the X-ray energy and gradients using the ML[27] or MLHL[28] target functions. Phenix was also used to compute $2mF_o – DF_c$ (2mFo-DFc) maps for real-space modeling and refinement in Rosetta; this can optionally include density modification in RESOLVE[29]. B-factor refinement was performed by *phenix.refine*[9].

The refinement script used in Rosetta consists of the following steps:

- Three cycles of side-chain optimization, followed by reciprocal-space torsion-angle minimization;
- Five cycles of side-chain optimization, followed by both real-space and reciprocal-space torsion-angle minimization;
- Two cycles of side-chain optimization, followed by Cartesian reciprocal-space minimization.

Each step also starts with the calculation of a new σ_A-weighted[30] $2mF_o – DF_c$ electron density map; this map—together with the Rosetta energy function—is used for side-chain optimization and (in some cycles) real-space refinement. Reflections flagged for cross validation[31] are replaced by DF_c to avoid bias[9]. By default, the grid spacing for the CCP4-format maps[32] was $d_{min}/2$. A single macrocycle of individual B-factor refinement was performed by *phenix.refine* at the end of each step. To ensure consistent calculation of the scattering contribution from bulk solvent and hydrogen atoms, the Rosetta models were run in *phenix.refine* for one cycle with a null strategy to recalculate R factors after refinement. The complete XML script is provided in **Supplementary Figure 1**.

To counter refined model variation in Rosetta-Phenix (typically 3–6% R_{free} variation between trajectories, but over 25% in extreme cases; see **Supplementary Fig. 6**), we ran multiple independent refinements in parallel and selected the result with the lowest R_{free}—a process similar to the protocol used for DEN refinement[2]. While this potentially biases an important validation statistic, in practice we found that for the test cases described here, only five runs were required to obtain adequate sampling, with an overall runtime comparable to that of DEN refinement in CNS. If a fully unbiased R_{free} statistic is desired, then the procedure could be carried out using a second fully free test set[33].

Refinement in Phenix. Coordinate and individual B-factor refinement were performed for 20 macrocycles, with automatic optimization of restraint weights using a grid search[34]. Only the default stereochemistry restraints were applied[35,36]. An alternate 'optimized' protocol, shown only in **Supplementary Tables 2** and **3**, was also run with 20 cycles of simulated annealing, using reference restraints derived from the starting structure.

Refinement in CNS. DEN refinements were performed as described[2], using a grid search to optimize the *gamma* and *w_den* parameters. Because the DEN protocol in CNS uses grouped B-factor refinement, additional individual B-factor refinement and bulk-solvent correction was performed in Phenix to obtain R factors comparable to the other methods.

Refinement in REFMAC. REFMAC5 refinements were run for 100 cycles, using automatic weighting and jelly-body restraints with $\sigma = 0.02$. R factors were then recalculated using phenix.refine to ensure consistent bulk solvent handling.

Evaluation of results. All refined models were validated using MolProbity[16] as implemented in the Phenix suite. R.m.s. deviations to the published structures were calculated using *phenix.superpose_pdbs*, including all non-hydrogen backbone atoms and side chains out to the $C\gamma$ atom where present.

High-resolution data set. The HiQ54 data set[37] consists of 54 non-redundant, monomeric, atomic-resolution structures (0.8–1.4 Å) with MolProbity score ≤1.4, near-zero geometry outliers and no large, tightly bound ligands. Structures were prepared for Rosetta refinement by removing all ligands except waters and all alternate conformations and then refining in *phenix.refine* for three macrocycles with all default parameters. Rosetta-Phenix refinements were performed with explicit hydrogens using a streamlined protocol consisting of only the final two Cartesian-minimization cycles. The refined structures were compared to the starting models by removing hydrogen atoms and re-running *phenix.refine* on both input and output models with a null strategy as above.

22. McCoy, A.J. *et al. J. Appl. Crystallogr.* **40**, 658–674 (2007).
23. Bunkóczi, G. & Read, R.J. *Acta Crystallogr. D Biol. Crystallogr.* **67**, 303–312 (2011).
24. Oeffner, R., Bunkóczi, G. & Read, R.J. *Computat. Crystallogr. Newslett.* **3**, 5–10 (2012).
25. Abrahams, D. & Grosse-Kunstleve, R.W. *C/C++ Users J.* **21**, 29–36 (2003).
26. Afonine, P.V., Grosse-Kunstleve, R.W. & Adams, P.D. *Acta Crystallogr. D Biol. Crystallogr.* **61**, 850–855 (2005).
27. Lunin, V.Y., Afonine, P.V. & Urzhumtsev, A.G. *Acta Crystallogr. A* **58**, 270–282 (2002).
28. Pannu, N.S., Murshudov, G.N., Dodson, E.J. & Read, R.J. *Acta Crystallogr. D Biol. Crystallogr.* **54**, 1285–1294 (1998).

29. Terwilliger, T.C. *Acta Crystallogr. D Biol. Crystallogr.* **56**, 965–972 (2000).
30. Read, R.J. *Acta Crystallogr. A* **42**, 140–149 (1986).
31. Brünger, A.T. *Nature* **355**, 472–475 (1992).
32. Winn, M.D. *et al. Acta Crystallogr. D Biol. Crystallogr.* **67**, 235–242 (2011).
33. Kleywegt, G.J. *Acta Crystallogr. D Biol. Crystallogr.* **63**, 939–940 (2007).

34. Afonine, P.V., Echols, N., Grosse Kunstleve, R.W., Moriarty, N.W. & Adams, P.D. *Computat. Crystallogr. Newslett.* **2**, 99–103 (2011).
35. Engh, R.A. & Huber, R. *Acta Crystallogr. A* **47**, 392–400 (1991).
36. Vagin, A.A. *et al. Acta Crystallogr. D Biol. Crystallogr.* **60**, 2184–2195 (2004).
37. Leaver-Fay, A. *et al. Methods Enzymol.* **523**, 109–143 (2013).